Available online at www.sciencedirect.com

ScienceDirect

Procedia Structural Integrity 18 (2019) 63–74

Structural Integrity Procedia

www.elsevier.com/locate/procedia

25th International Conference on Fracture and Structural Integrity

A Numerical and Experimental Analysis of Inconel 625 Electron-Beam Welding – Thermal Aspects

Luca Romanin[a]*, Paolo Ferro[a], Franco Bonollo[a], Filippo Berto[b]

[a]*University of Padova, Depatement of Engineering and Management, Stradella San Nicola 3, 36100 Vicenza, Italy*
[b]*NTNU, Department of Mechanical and Industrial Engineering, Richard Birkelands vei 2b, 7491 Trondheim, Norway*

Abstract

Inconel 625, a nickel based superalloy, finds application in many fields. It is known to have a good weldability and it is often used in the as-welded conditions, heat treatments could be necessary to relief stresses. Numerous variables are known to affect the residual stresses field: welding process, joined geometry and clamping conditions. Since experimental measurements based on X-ray diffraction are not straightforward, expensive experimental work could be substituted by numerical simulation. Before performing an elastoplastic simulation, thermal analysis results are needed, first.
This paper focus on the thermal analysis procedure. The analysis has been validated by means of macrographs and with thermocouples data. The heat source was successfully modelled using a superimposition of a spherical and a conical shape heat source with Gaussian power density distribution in order to reproduce the nail shape of the fusion zone. Heat source parameters were chosen so that the model would match with experimentally determined weld pool shape and temperatures. Preliminary results of the metallurgical analysis are also presented.

Peer-review under responsibility of the Gruppo Italiano Frattura (IGF) ExCo.

Keywords: Inconel 625; Electron Beam Welding; Thermocouples; Thermal analyisis

* Corresponding author.
E-mail address: luca.romanin@phd.unipd.it

2452-3216
Peer-review under responsibility of the Gruppo Italiano Frattura (IGF) ExCo.
10.1016/j.prostr.2019.08.140

1. Introduction

Inconel 625 finds application in the aerospace industry and in those sectors where an excellent combination of corrosion resistance and high strength is needed. Common applications include turbine shroud rings, aircraft ducting and exhaust systems, valve seats, furnace muffles, motorsport exhaust and clamps. Due to the high nickel content (58wt%), Inconel 625 has good resistance to pitting and crevice corrosion and it is immune to chloride-induced stress corrosion cracking. Strengthening is performed by solid-solution hardening.

In addition, it has a good weldability and it is often used in the as-welded conditions. Problems arises when larger grain size are utilized in order to increase creep resistance. Weldability, as well as ductility, is reduced and low heat input methods have to be utilized. Since the small zone of grain growth in HAZ does not appreciably reduce weld strength, post weld heat treatments are not required. However, they could be utilized to relief stresses, remove cold work or dissolve carbides. In this latter case, solution annealing in the range 1095-1205°C is performed causing recrystallization and dissolution of $M_{23}C_6$ carbides formed during weld cooling.

Residual stress distributions are known to depend on the chosen welding process, joint geometry and clamping conditions. Experimental measurements based on X-ray diffraction are not straightforward; for this reason, expensive experimental work could suitably be substituted by numerical simulations. Residual stresses are then calculated enabling to determine if post weld heat treatments are necessary or not. To perform an elastic-plastic simulation, thermal analysis results are needed, first. This paper focuses on the thermal analysis procedure and its correlation with experimental metallographic results.

The chosen welding process is the Electron Beam Welding (EBW), a high-energy-density fusion process in which the kinetic energy of accelerated electrons are converted into thermal energy as they penetrate into the workpiece. It is utilized because the weld quality is equal or superior to that produced by arc welding and because the fusion zone (FZ) is smaller compared to that produced by arc welding.

Some authors already tackled EBW, each one with different approaches. Ferro et al. (2005) investigated the electron beam welding of Inconel 706, they found a good agreement between thermal-mechanical analysis and experimental data. The numerical model was helpful in correlating microfissures occurring at the grain boundaries, under the nail head of the bead, with process parameters. They carried out the thermal analysis by superimposing a spherical and conical heat source.

Also Laki et al. (2011) studied the EBW of 30HGSA steel using only a conical heat source. They also found good consistency with empirical data. In a more recent investigation, Laki et al. (2014), from a series of 49 weld experiments, created a Partial Least Square model of the FZ and subsequently defined the heat source utilizing mesh segments and constant power density on each segment.

A move from the phenomenological approach has been done by Palmer et al. (2009) when they simulated the EBW of 304L stainless steel. They included thermal conductivity and viscosity to account for enhanced heat and mass transfer due to turbulence in the weld pool and found that convective heat transfer was very significant in determining the weld geometry. However, this type of analysis is not convenient for a subsequent mechanical analysis because it involves results mapping from a Finite Volume Method to a Finite Element Method code.

In this work, a numerical model of EBW of Inconel 625 has been developed. The phenomenological approach proposed is based on the calibration of the source parameters on the basis of macrographs and temperature measurements by means of thermocouples. Experimental and calculated results were in good agreement and open the way to a future mechanical analysis. The obtained results will be used also for a further development of the thermal-metallurgical model that includes phase precipitation.

Nomenclature

HAZ	Heat Altered Zone
EBW	Electron Beam Welding
FZ	Fusion Zone
GTAW	Gas tungsten Arc Welding

EDS	Energy Dispersive X-ray Spectrometry

2. EBW parameters optimization

EBW parameters have been optimized by welding four plates made of Inconel 600 which has lower Chromium and higher Nickel content than Inconel 625. Like Inconel 625, it is a nickel-based solid-solution superalloy. Its use was considered acceptable because it served only as a test to obtain a good quality full penetration butt weld.

For every pre-test, the electron beam spot was fixed at 1.5 mm of diameter and the heat source speed at 12 mm/s. at the same time all other parameters, with the exception of the beam current, have been kept constant. The parameters utilized could be seen in Table 1.

Table 1. EBW parameters optimization

	Accelerating voltage [kV]	Beam current [mA]	Focus current [mA]	Spot diam. [mm]	Freq. [Hz]	Speed [mm/s]
Pre-Test 1	150	17	347	1.5	300	12
Pre-Test 2	150	16	347	1.5	300	12
Pre-Test 3	150	12	347	1.5	300	12

Using 16 and 17 mA proved enough to obtain full penetration, however the heat input was too high, causing a highly irregular weld seam. Using lower currents, instead, 12 and 14 mA, full penetration was not reached but a good quality weld bead was obtained at the upper surface. It was chosen to use a current of 15 mA to perform testing.

3. Material and experimental procedure

The chemical composition of the specimens has been measured by EDS and is summarized in Table 2 for the specimen labelled “Test 1”.

Table 2. Chemical composition calculated by EDS on specimen Test 1 (wt%)

Ni	Cr	Fe	Mo	Nb+Ta	C	Mn	Si	Al	Ti	Co
58.30	20.39	3.94	8.91	3.76			0.32		0.22	

Every test consists of welding two plates (dimensions:16 mm x 72 mm x 2.5 mm) by means of EBW as in Figure 1. Since no filler material has been used, the joining edges have been prepared to obtain the best contact.

To validate thermal analysis results, in the specimen labelled “Test 4”, two K-type thermocouples have been inserted at 2.5 mm and 6 mm from the weld seam, as shown in Figure 1. The holes with a diameter of 1 mm have been realized with Electro Discharge Machining. Picotech TC-08 Termocouple Data Logger has been utilized to record data.

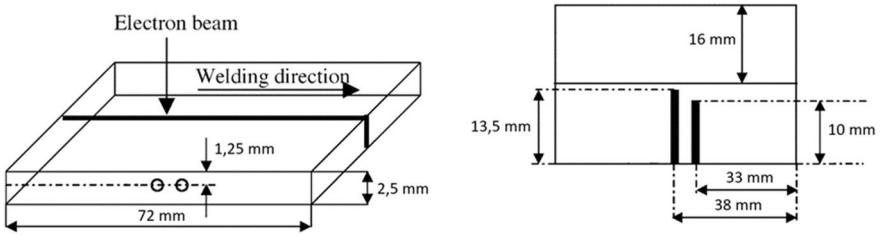

Fig. 1. (a) side view and (b) top view of the specimen. Holes for the thermocouples could be noted in both schemes.

Half of the specimens (samples used for Test 1 and 2) have been stress relieved before welding, in order to study, in a future work, the influence of pre-existing residual stresses on residual stress filed induced by welding.

Stress reliving consisted in keeping the specimens at 870 °C for around 40 minutes, then they have been cooled down to 630 °C in the heat furnace, subsequently to 570 °C opening the furnace door and finally a slow cool down in air. The steps are summarized in Table 3.

Table 3. Stress relieving heat treatment before welding for Test 1 and 2

t [min]	T [°C]	
0	20	Heating
5	870	
40	870	
63	630	Furnace cooling
68	570	Door open
100	100	Air cooling
101	20	Water cooling
0	20	Heating

Inconel 625 sheets were first clamped as shown in Fig. 2 and then tack welded in six points, one every 10 mm, in order to avoid the creation of a gap due to thermal expansion. Weld tacking increased also the overall specimen temperature as it can be seen in Fig. 13, in a similar way of a preheat because of the small specimens' mass.

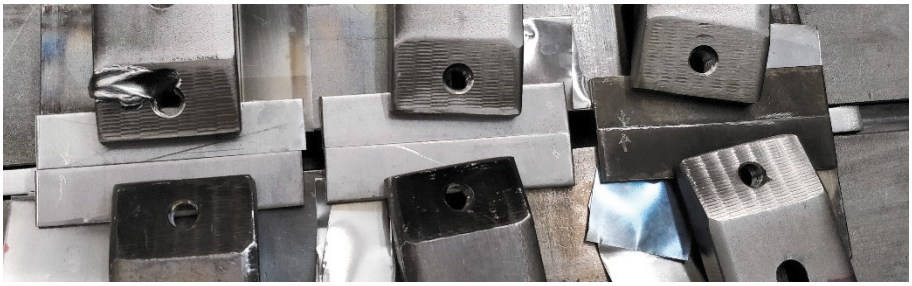

Fig. 2. Clamping configuration

Tests have been conducted according to parameters defined in Table 4, in a vacuum chamber with a pressure of 4 10^{-4} mbar.

Table 4. EBW test parameters

	Accelerating voltage (kV)	Beam current (mA)	Focus current (mA)	Spot diam. (mm)	Freq. (Hz)	Speed (mm/s)	Notes
Test 1	150	15	347	1.5	300	12	Stress relived
Test 2	150	15	347	1.5	300	12	Stress relived
Test 3	150	15	347	1.5	300	12	
Test 4	150	14,5	347	1.5	300	12	Thermocouples

The tests did not obtained full penetration in the first 10 mm of the welding line; as a matter of fact, a trapezoidal velocity profile should have been utilized. However, starting and ending point are not taken into account in this work. In Test 2 and 3, the current proved to be too high and a crater has formed at about 2/3 of the welding line. Because starting and ending lack of full penetration could be neglected, for the last specimen with thermocouples the current has been slightly lowered to 14.5 mA.

4. Preliminary metallurgical results

Data enabling to validate phase models is expected to be found. As-delivered conditions were analysed by using the parent material of specimen named “Test 3” while the results of the stress relief treatment were analysed by using parent material of specimen named “Test 1”.

Phases precipitation is not yet included in thermal analysis because thermal properties are not affected by precipitates. With the scope of predicting phase precipitation Wang et al. (2008) developed a complex model requiring data such as diffusion coefficients of elements, surface energies, interface kinetic coefficients and driving forces for phase transformations. To overcome the limitation due to the high number of material data required, Ferro (2013) proposed a semi-empirical model derived from Johnson-Mehl-Avrami-Kolmogorov equation that includes an impingement factor taking into account particle size distribution and interaction with undissolved particles.

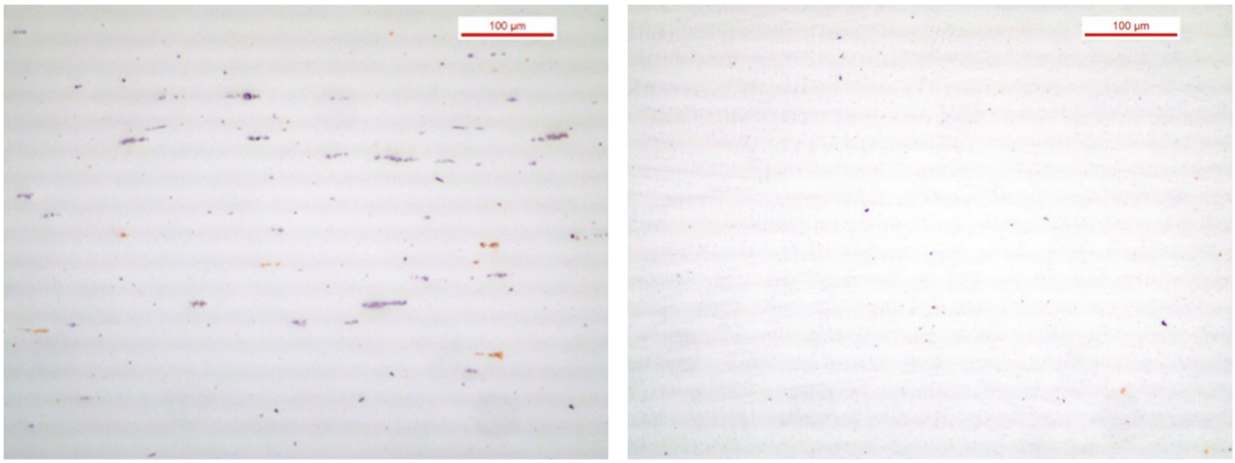

Fig. 3. (a) Phases in base material in Test 1 (100x magnification). (b) Phases in fused zone (100x magnification)

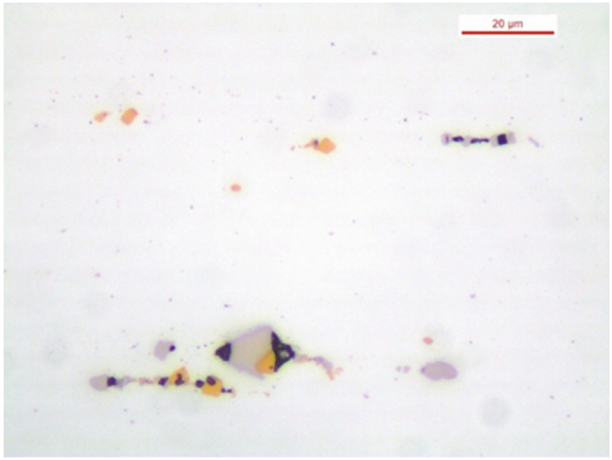

Fig. 4. Phases in base material in Test 3 (500 x magnification)

Specimens named “Test 1” and “Test 3” have been primarily analyzed under optical microscope to characterize their microstructure and record differences. In both specimens, a homogenous presence of precipitates could be observed in the base material while it is not present in the weld bead as is shown in Figure 3 (b). Both the macrographs of the specimens are presented with a 12.5x magnification without etching, in this way grains boundaries are not

visible, and precipitates are more evident. By increasing the magnification, two types of precipitates could be classified by their shape, one developing in the direction of rolling and present only in the parent metal and the other one with a rounded shape and present both in the parent metal and in the FZ.

The first one is in the order of 10 μm long while the latter is around 0.1 μm large. At the optical microscope no appreciable difference between the stress relived specimen (Test 3) and the as-received specimen could be noted in the parent material.

5. Numerical model

A non-linear thermal transient analysis of the welding process has been performed. The fast motion and extremely fine focus of the heat source cause severe temperature gradients which have to be captured by a fine mesh and a small time-step. Even though a very fine mesh is not required in the thermal analysis, the more stringent requirements of the mechanical analysis constrain the mesh size. Taking advantage of geometrical and load symmetry only one plate has been modelled. A fixed time step of 0.05 s has been chosen when the heat source was moving inside the specimen.

One of the objectives is to find the computational cheapest numerical model that could replicate experimental results. Thermal results are going to represent the input for a planned mechanical analysis, which is known to be more computational expensive.

The thermal model has been validated using data of the specimen named “Test 3” in which two thermocouples have been inserted and a macrograph has been obtained from the middle section (Fig. 9).

5.1. Mesh

40000 ca. 3D linear elements have been utilized. The mesh has been graded both in the transversal and in the longitudinal direction to optimize the number of elements. On the symmetry plane, along the thickness, 8 elements of around 0.3 mm have been used as it can be seen in Figure 5. Moving far from the weld bead, gradually, only 4 elements along the thickness have been used.

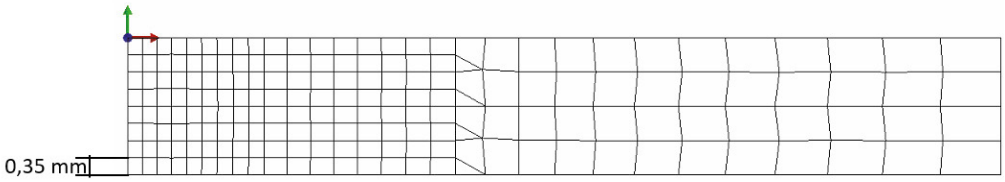

Fig. 5. Cross section of the mesh

In the longitudinal direction the mesh is finer at the start and end of the weld seam while coarser in the middle where thermal condition can be considered quasi-stationary. For this reason, in the longitudinal direction, a parabolic bias has been imposed to have a finer mesh in the starting and ending region because of higher gradients due to the start and stop of the weld. Elements size ranges from 0.17 mm (welding start/end) to 0.77 mm in the middle, where the heat conduction could be considered stationary along the longitudinal direction.

5.2. Boundary and Initial conditions

Heat loss have been taken into account considering thermal radiation, using the Stefan-Boltzman law, and an equivalent value for convection. Even if EBW was performed in vacuum, convection has been artificially introduced to take into account the heat dissipated by conduction from the clamps. Because of the small dimensions of the specimen the effect of the clamps is non negligible, the advantage of utilizing the convection coefficient is avoiding to model contact resistance which would have required a phenomenogical calibration and introduced another source of error. The value of the convection coefficient was empirically determined to be 10 W/m^2, while the ambient temperature has been fixed to 25°C.

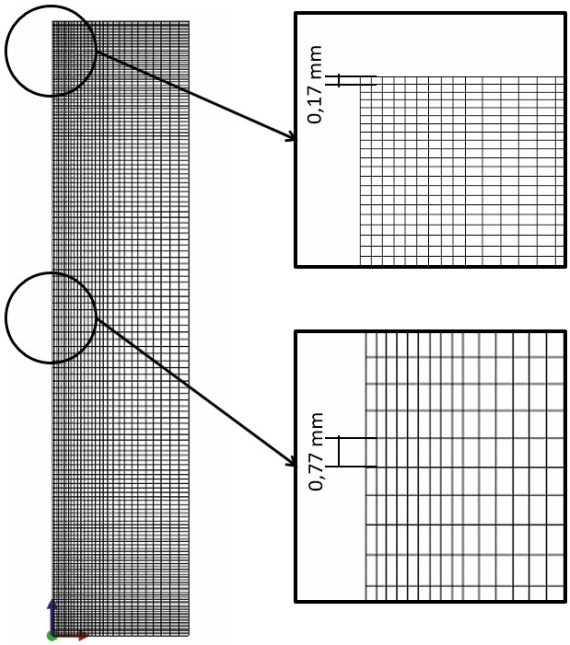

Fig. 6. Details of mesh extrusion at various points

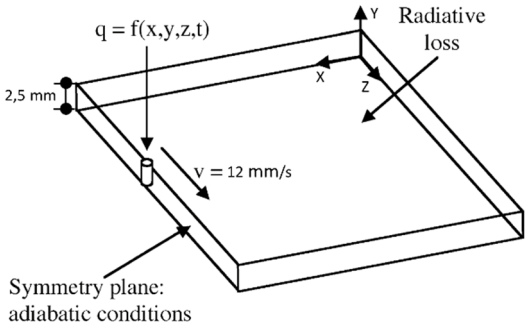

Fig. 7. Boundary conditions on the modelled half specimen

The initial temperature for the specimen has been set to 95°C, as it can be noted from thermocouples data in Figure 13 and 14. The reason for the increased initial temperature is due to tack welding in several points.

5.3. Modelling of the heat source

During EBW, in the beam impingement zone, a portion of material evaporates creating a cavity containing metallic plasma because of the process high power densities. Various authors have studied the keyhole formation and evolution in EBW or laser welding by using CFD in order to predict gas porosity. In this case, a phenomenological approach has been preferred that uses thermocouple data and micrographs of the fusion zone; in this way the mechanical simulation is more straightforward. The characteristic nail shape has been simulated by superimposing a spherical and a conical heat source.

The spherical heat source has a constant power density distribution (q_0) in the range between r = 0 and r = R1 (inner radius) and a linear power density decreasing from R1 to R2 (outer radius).

$$\begin{cases} q_0 & if\ 0 < r < R1 \\ q_0 \frac{R2-r}{R2-R1} & if\ R1 \le r \le R2 \end{cases} \quad (1)$$

The conical heat source has instead a Gaussian power density distribution centered in its axis:

$$q_2 = q_{2,max} e^{-\frac{r^2}{r_0^2}} \quad (2)$$

Where $r^2 = (z - v\,t)^2 + x^2$ and $r_0 = R_e - (R_e - R_i)(y_e - y)/(y_e - y_i)$ for $y_i < y < y_e$. The heat source moves along z axis while the thickness is along y axis.

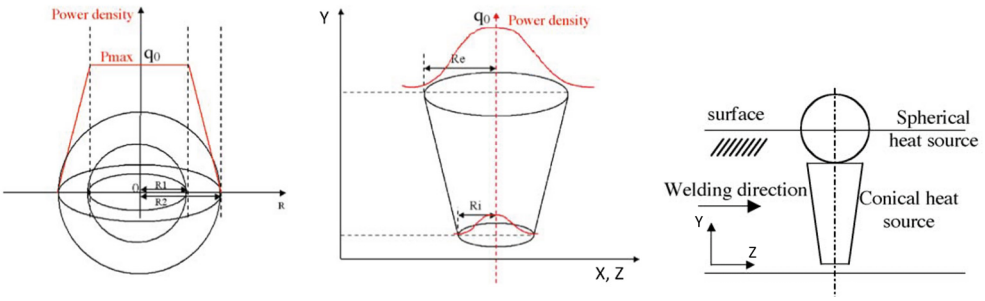

Fig. 8. (a) Spherical heat source; (b) Conical heat source; (c) Superimposition of heat sources.

Heat source parameters have been chosen comparing experimental results with the numerical model. The parameters obtained for the specimen called 'Test 4' are given in Tables 5 and 6 for the spherical and conical heat source respectively.

Table 5. Spherical heat source parameters

q_0 [W/mm^3]	R1 [mm]	R2 [mm]
260	0.5	1.6 mm

Table 6. Conical heat source parameters

q_0 [W/mm^3]	R_i [mm]	R_e [mm]	y_i [mm]	y_e [mm]
90	0.9	0.9	-1.5	-2.5

As observed in Figure 9, comparing the FZ coming from numerical model with that obtained in the experiment, the phenomenological approach has given good results.

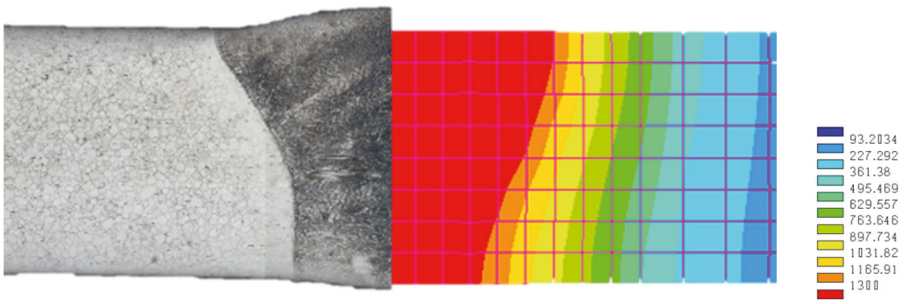

Fig. 9. Comparison of the measured and predicted fusion profile for the butt-welded plates in the middle section. Temperatures are expressed in °C

The characteristic nail shape could be noted also from a 3D isotherm plot. The reference temperature for the fused zone is 1300°C and is represented by the red isothermal surface of Figure 10.

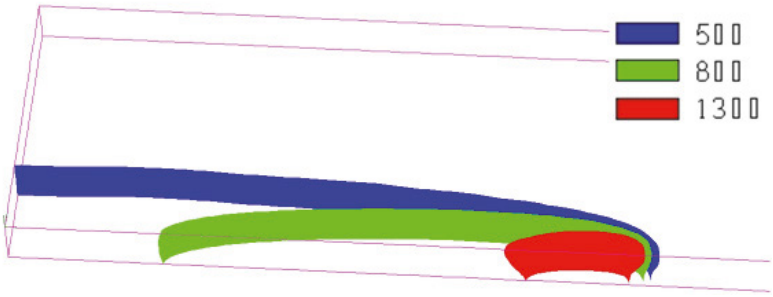

Fig. 10. Isothermal surfaces for 1300°C (fused material), 800°C and 500°C.

5.4. Material properties

Non-linear thermal properties have been used. Thermal conductivity, density and specific heat versus temperature exhibit a non-linear behavior. Precipitates that forms during cooling have no effect on thermal properties. Data is available up to 1300° C even if the material undergoes higher temperatures, reaching evaporation. For the sake of simplicity, the effects of phase change from solid to liquid have not been included in the model. As a matter of fact, it has been found numerically that the effect of latent heat to liquid is neglectable for the high energy densities involved in EBW.

Thermal properties as a function of temperature are reported in Figure 11.

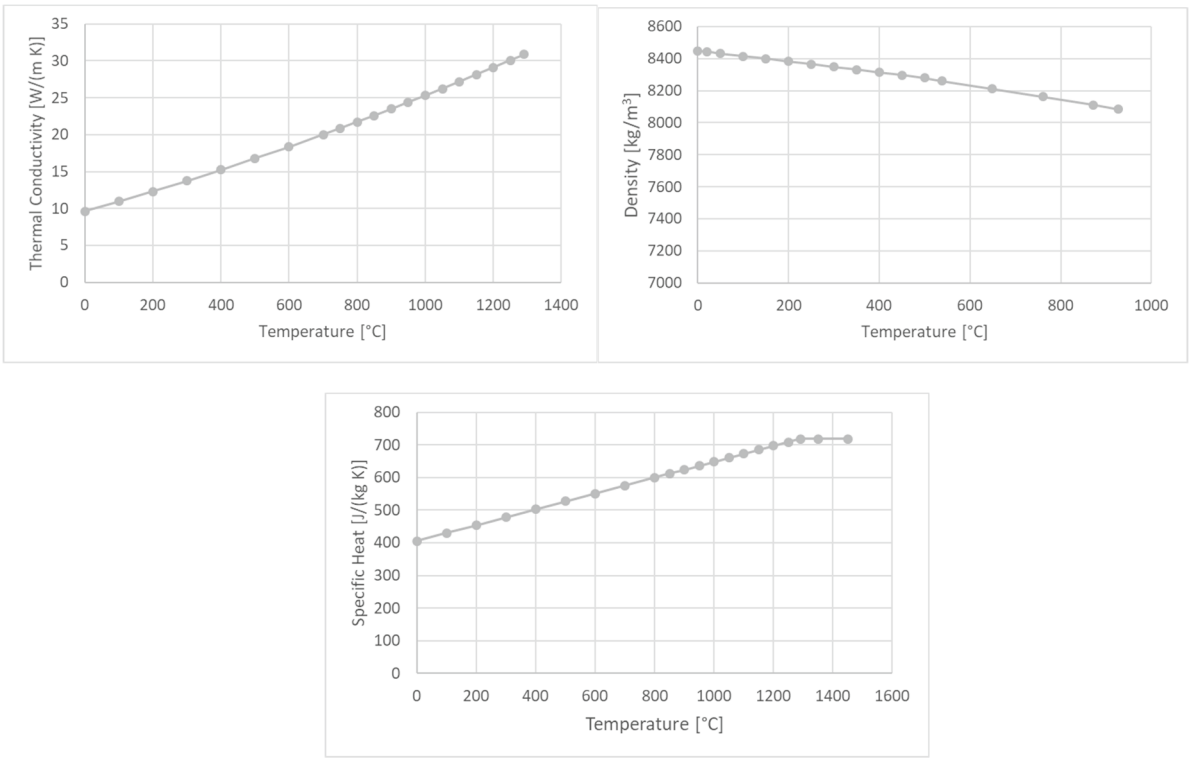

Fig. 11. Thermal material properties for INCONEL 625 (a) Thermal conductivity; (b) Density; (c) Specific heat.

6. Thermal results

The specimen ‘Test 4’ has been equipped with thermocouples inserted at various distance from the weld seam in the middle of the thickness. Experimental results are thus used as a validation for the numerical model.

The thermocouples are positioned at 2.5 mm and 6 mm from the weld seam as shown in Figure 1. The effect of two subsequent tack welding could be noted from both the thermocouple data in the time frame before the EBW start. It could be noted that the temperature difference of the thermocouples in the tack welding phase is contained. In addition, the weld pass is going to re-melt the tack welded spots resetting the residual stress field. The mechanical analysis could then neglect the effect of tack welding.

The shape prediction of the FZ is shown in details by the contour plot of the specimen top view in Figure 12 (a) and by the multiple cross sections in Figure 12 (b).

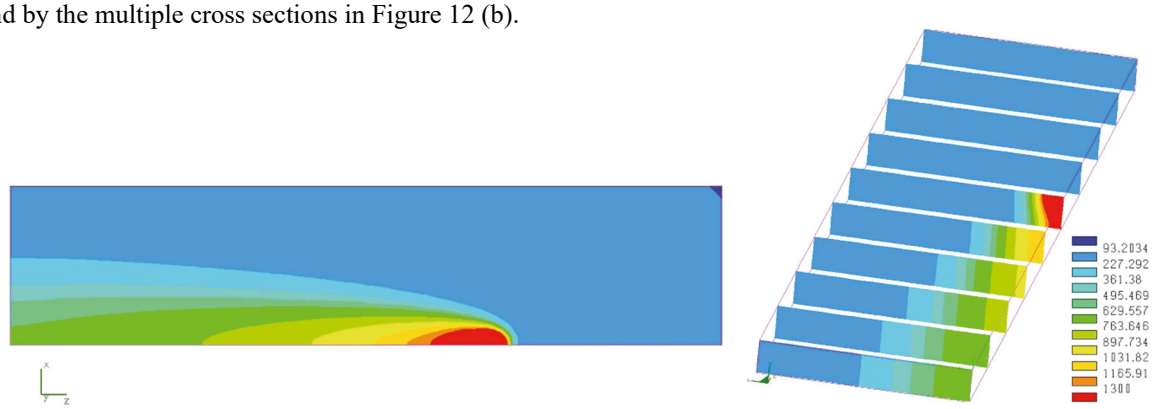

Fig. 12. (a) Top view of the calculated thermal field. (b) Cross sections

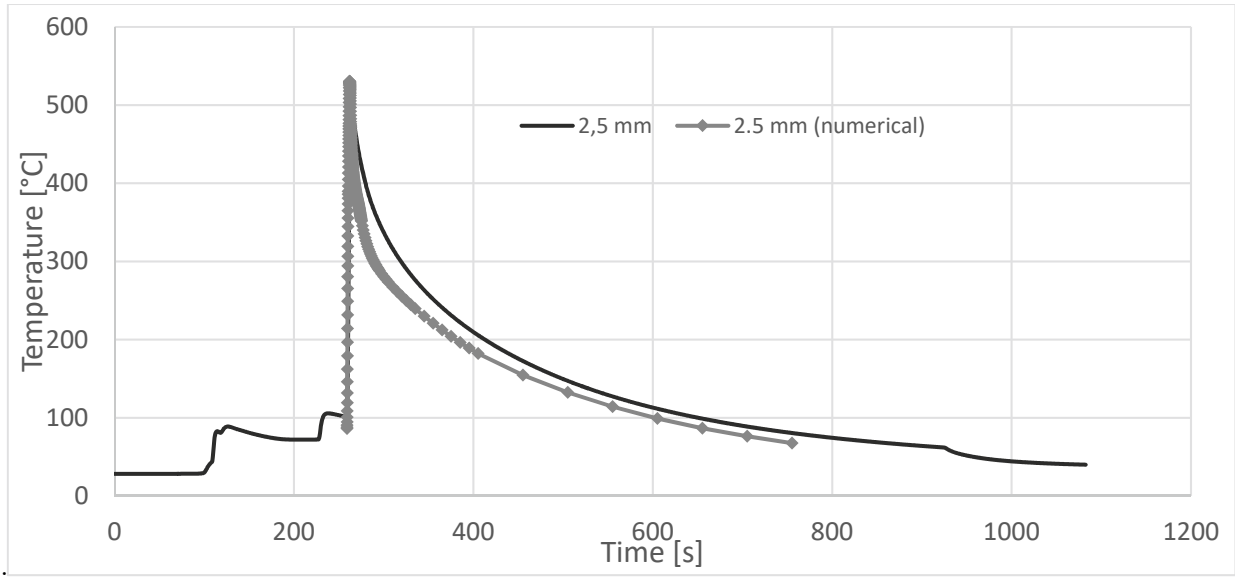

Fig. 13. Comparison of thermocouple (solid black line) and numerical results (grey line). The thermocouple was positioned at 2.5 mm from the joining edges.

Comparing the results at 6 mm, the most far from the weld bead, the numerical peak is reached at 376 °C versus 390 °C read by the thermocouple. The cooling rate has been successfully predicted meaning that boundary conditions for convection and radiation are in agreement with experimental data.

Nearer the weld bead, in correspondence of the 2.5 mm thermocouple, the numerical temperature peak is 544°C against the experimental value of 485°C. However, the numerical and experimental cooling rates are quite similar. A much finer mesh is not recommended as a mechanical analysis would result too heavy to be resolved. Moreover, to obtain thermal convergence, very often, a very fine mesh is not needed. At the same time, increasing the time step produces no improvement.

The reason of the little differences in cooling rate could be the presence of transport phenomena in the molten region that increase the dissipated heat and that cannot be taken into account in the phenomenological approach. Another reason could stay in the non-linearity of the emissivity coefficient that is not included for sake of simplicity. Irradiation is the largest heat transfer phenomenon at high temperature because EBW is performed in vacuum. A higher emissivity coefficient for high temperature could justify the steeper cooling rate and still keeping the correct behavior of the thermocouple more far from the weld bead. From the work of Palmer et al. (2009) it seems more plausible that neglecting convective heat transfer in the FZ is causing the small discrepancies in Figure 14. The thermal conductivity should be adjusted for temperatures that are higher than melting temperature.

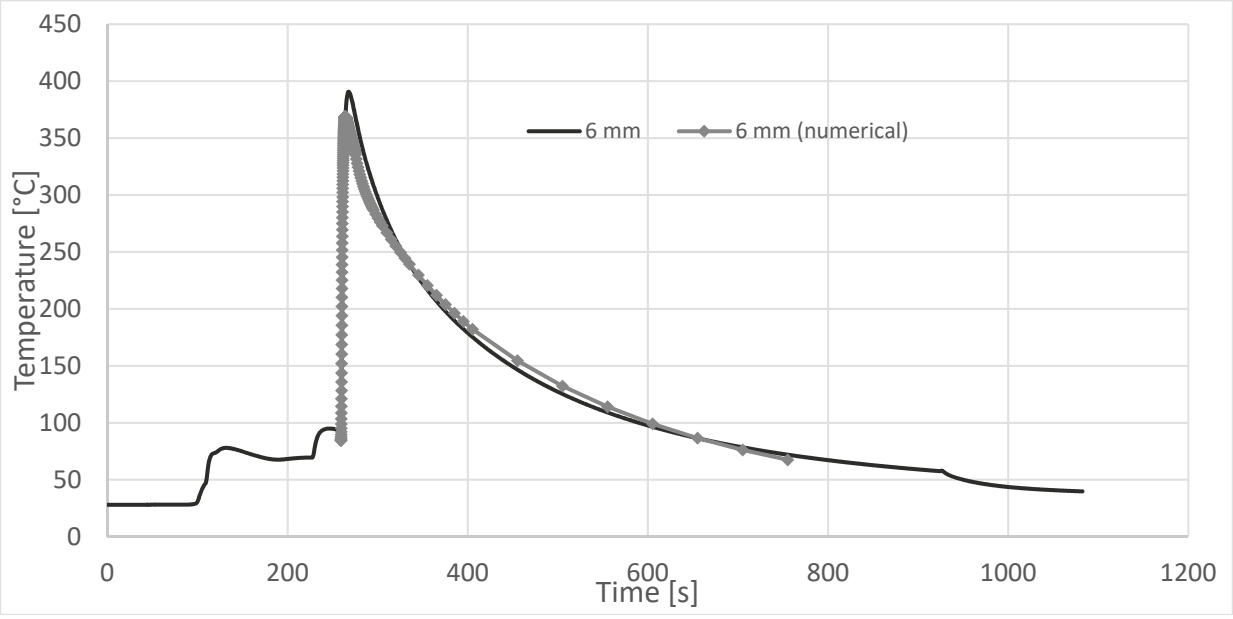

Fig. 14. Comparison of thermocouple (solid black line) and numerical results (grey line). The thermocouple was positioned at 6 mm from the joining edges.

7. Conclusions

A thermal characterization of the Inconel 625 EBW process was carried out. After having optimized by experiments the welding parameters, a thermal model for the heat source has been calibrated. Two heat source functions have been superimposed. A spherical source in the upper part of the sheets takes into account the wide fusion zone caused by the electron beam defocalization, while a conical source models the penetration depth of the electron beam.

It has been found a closed match between the experimental and numerical FZ shape. At the same time, thermocouple data has been found close to the numerical values. For the thermocouple positioned at 6 mm from the weld bead the match is almost exact meaning that thermal boundary conditions are chosen correctly.

Thermal results have been demonstrated to be in close agreement with the experiment. They represent the subsequent input for a mechanical analysis for the numerical prediction of residual stress fields.

Acknowledgements

The authors gratefully acknowledge the experimental support provided by Zanon S.p.A., Schio (VI), Italy.

References

Ferro, P., Zambon, A., Bonollo, F. (2005). Investigation of electron-beam welding in wrought Inconel 706 — experimental and numerical analysis, 392, pp. 94–105, Doi: 10.1016/j.msea.2004.10.039.

Lacki, P., Adamus, K. (2011). Numerical simulation of the electron beam welding process, Comput. Struct., 89(11–12), pp. 977–85, Doi: 10.1016/j.compstruc.2011.01.016.

Lacki, P., Adamus, K., Wieczorek, P. (2014). Theoretical and experimental analysis of thermo-mechanical phenomena during electron beam welding process, Comput. Mater. Sci., , pp. 1–10, Doi: 10.1016/j.commatsci.2014.01.027.

Palmer, T.A., Elmer, J.W., Debroy, T. (2009). Heat Transfer and Fluid Flow during Electron Beam Welding of 304L Stainless Steel Alloy ABSTRACT, 88(March),.

Zhou, N., Ma, N., Xu, D.S., Yang, R., Payton, E.J., Wang, G., Wang, Y., Mills, M.J. (2008). Simulation study of effects of initial particle size distribution on dissolution, Acta Mater., 57(2), pp. 316–25, Doi: 10.1016/j.actamat.2008.09.010.

Ferro, P. (2013). A dissolution kinetics model and its application to duplex stainless steels, Acta Mater., 61(9), pp. 3141–7, Doi: 10.1016/j.actamat.2013.01.034.